Impact of Superconducting Fault Current Limiter with Delayed Recovery on Transient Rotor Angle Stability

Rohit S. Thute, Himanshu J. Bahirat, and S. A. Khaparde

***Abstract*—A fault current limiter (FCL) is an economical option to limit the increased fault current levels, which may also improve the rotor angle stability. Previous studies on this topic mainly focused on the FCLs with quick recovery and concluded that the FCL improves the rotor angle stability. However, some commercially available FCLs have delayed recovery, which may pose different challenges and need to be studied. This paper studies the impact of a superconducting fault current limiter (SCFCL) with delayed recovery on transient rotor angle stability. This paper first develops an analytical understanding of the stability of a system with SCFCL using the equal area criterion. Later, time-domain simulations are employed to demonstrate the impacts of the SCFCL on the rotor angle stability of a single-machine infinite-bus system. The results show that the SCFCL with delayed recovery leads to rotor angle instability in some cases.**

***Keywords*—Critical clearing time, Superconducting fault current limiter, Recovery, Transient rotor angle stability.**

I. Introduction

Increasing energy demand requires adding new energy resources to the existing grid, which increases its fault levels. The increase in fault levels beyond equipment ratings leads to equipment failures [1]. These situations demand the up-gradation of the system equipment to ensure reliable service, which may not be planned by the utility. Such unplanned up-gradation of the system equipment has economic implications for the utility. One economical solution to this problem is to use a fault current limiter (FCL), which appears in the system only during faults and limits the fault current by injecting impedance in the fault path. These FCLs are installed to limit the fault levels below the ratings of existing equipment. One such FCL is the superconducting fault current limiter (SCFCL). The SCFCL application studies involve limiting fault levels at a particular bus in the grid [2], at branches connecting two areas of the grid [3], at generating stations [4], and at distribution systems with distributed generators [5]–[7].

The rotor angle stability of the network depends on the fault location and severity, which makes it essential to study the impact of such FCL installations on the rotor angle stability. Literature [8]–[16] presents studies on the impacts of various SCFCLs on rotor angle stability. These studies conclude that the fault current limiting aspect of the SCFCL, which involves quickly limiting the fault current, improves the rotor angle stability of the system. Some studies, like [10]–[12], [17], [18], use this fact to decide the optimal location of SCFCL in the network to enhance rotor angle stability for various faults in the network. These studies can be divided into two groups based on the behavior of the SCFCL after fault inception. 1. The studies presented in [8]–[11], [17]–[19] consider SCFCL with quick recovery, which transitions from a high to low impedance state at fault clearing, 2. The studies presented in [14]–[16] consider special cases of SCFCL installation, where the SCFCL gets disconnected with the faulty network element. These studies do not consider SCFCL impedance in the network during the post-fault period, which is the case for SCFCLs with delayed recovery. Such SCFCL impedances in the post-fault period may adversely impact the transient rotor angle stability [20], [21].

Quick recovery of SCFCL is inherently possible in non-quench-type SCFCLs, such as iron core SCFCL, but not in the case of quench-type SCFCLs [22]. One such example of a quench-type SCFCL is a resistive SCFCL with a shunt reactor. This SCFCL consists of superconductors whose recovery time ranges from 1 to 5 s [23]. Hence, this SCFCL injects impedance in the network from fault inception to the successful recovery of the quenched superconductors. Some studies propose constructional modifications to avoid SCFCL impedance in the post-fault period. These studies include 1. the SCFCL with multiple SC elements in parallel [9], [17], [24], which may increase the cost of the SCFCL installation, and 2. the SCFCL with bypass circuit breaker [18], which makes it ineffective in case of back-to-back faults [14]. On the contrary, some commercially available transmission-grade quench-type SCFCLs do not employ these modifications and have a recovery time of 10 to 45 s [2], [25]. The impedance of such SCFCLs changes the power transfer in fault and post-fault periods. Since the power transfer in the post-fault period is crucial for the rotor angle stability, it is necessary to identify the impacts of SCFCL on rotor angle stability. The previously discussed studies on resistive SCFCL do not consider the recovery aspect of the SCFCL operation. Ref. [21] presents impact of inductive SCFCL with ferromagnetic core which have delayed recovery on transient stability. The inductive SCFCL are different from resistive SCFCL with shunt reactor, especially, in their recovery characteristics.

The contributions of this paper are as follows:

- a method to analyze the rotor angle stability of a system consisting of SCFCL with delayed recovery,

Authors are with Department of Electrical Engineering, Indian Institute of Technology Bombay, Mumbai, MH 400076 INDIA (e-mail of corresponding authors: rohitthute@ee.iitb.ac.in, hjbahirat@ee.iitb.ac.in).

Paper submitted to the International Conference on Power Systems Transients (IPST2023) in Thessaloniki, Greece, June 12-15, 2023.

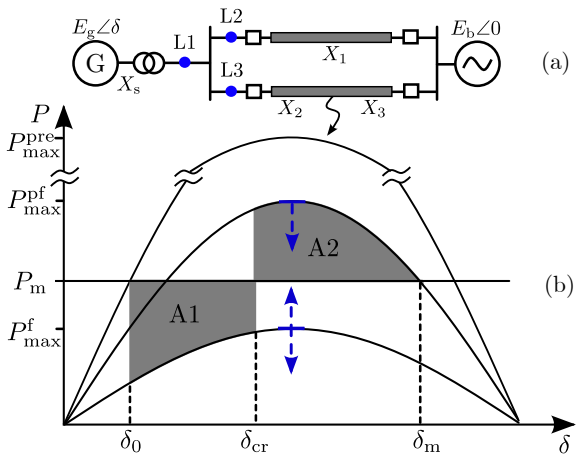

Fig. 1. (a) System with possible SCFCL locations, and (b) Power-angle curve with SCFCL considerations for studying first swing stability

- identification of conditions that adversely impact the rotor angle stability in the presence of SCFCL,
- a comparison of the system rotor angle stability for SCFCL with quick recovery and different SCFCLs with delayed recovery, and
- validation of conclusions presented in [21].

The rest of the paper is arranged as follows: Section II develops the mathematical understanding of transient rotor angle stability with SCFCL. Section III presents the test system and test cases considered in the paper. Section IV discusses the time-domain simulation results. Section V concludes the paper.

II. Transient Rotor Angle Stability of a System Consisting of SCFCL with Delayed Recovery

This section develops the problem understanding based on mathematical analysis. The analysis employs the equal area criteria [26] to comment on the impact of SCFCL with delayed recovery on the first swing stability of a system.

A. First Swing Rotor Angle Stability: Basics

Fig. 1a shows a system consisting of a synchronous generator connected to an infinite bus through two parallel transmission lines. The transient stability is analyzed for a line fault, as shown in Fig. 1a, which is cleared by tripping corresponding circuit breakers. For this analysis, each element is represented by respective reactances shown in Fig. 1a. Considering constant infinite bus voltage ($E_b\angle0$) and internal generator voltage ($E_g\angle\delta$) in Fig. 1a, the effective impedance between them (X_{tra}) dictates the maximum electrical power output (P_{max}) as given by (1).

$$P_{max} = \frac{E_g E_b}{X_{tra}} \tag{1}$$

The value of X_{tra} changes according to network impedances in pre-fault, fault, and post-fault periods. In the pre-fault period, X_{tra} is given by $\frac{X_1X_2}{X_1+X_2} + X_s$. The network modifies in fault and post-fault periods. The first row of Table I shows these networks in fault and post-fault periods with respective X_{tra} expressions. The X_{tra} expressions suggest that $P^{f}_{max} < P^{pf}_{max} < P^{pre}_{max}$, where P^{pre}_{max}, P^{f}_{max}, and P^{pf}_{max} represent P_{max} in pre-fault, fault, and post-fault periods, respectively.

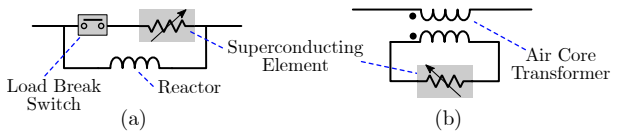

Fig. 2. Circuit representation of (a) resistive SCFCL, and (b) Air coil SCFCL.

Fig. 1b shows the corresponding power-angle curve representing $P = P_{max}\sin\delta$. The initial value of the rotor angle is $\delta_0 = \sin^{-1}(P_m/P^{pre}_{max})$ with the mechanical input power P_m and P^{pre}_{max} shown in Fig. 1b. Here, area A1 between P_m and $P^{f}_{max}\sin\delta$ represents the accelerating area. Area A2 between $P^{pf}_{max}\sin\delta$ and P_m represents the decelerating area with $\delta_m = \sin^{-1}(P_m/P^{pf}_{max})$. The equal area criteria, defined as (2), gives the critical clearing angle δ_{cr} for the fault. Eq. (3) defines δ_{cr} for given values of P_m, P^{f}_{max}, and P^{pf}_{max}. For constant P_m, any changes in P^{f}_{max} and/or P^{pf}_{max} modify the value of δ_{cr}.

$$\int_{\delta_0}^{\delta_{cr}} (P_m - P^{f}_{max}\sin\delta)d\delta = \int_{\delta_{cr}}^{\delta_m} (P^{pf}_{max}\sin\delta - P_m)d\delta \tag{2}$$

$$\cos\delta_{cr} = \frac{P_m(\delta_m - \delta_0) + P^{pf}_{max}\cos\delta_m - P^{f}_{max}\cos\delta_0}{P^{pf}_{max} - P^{f}_{max}} \tag{3}$$

B. Impact of SCFCL with Delayed Recovery

Fig. 2a shows the SCFCL under study. The SCFCL has a negligible impedance in pre-fault condition, which suggests no change in P^{pre}_{max}. During a fault, the load break switch disconnects the superconducting element, and the shunt reactor dominates the SCFCL impedance. The load break switch remains open till the recovery of the superconducting element, which spans beyond the fault period. The SCFCL impedance modifies the network impedance during the fault and the post-fault period. Hence, their combined effect must be considered to analyze the transient stability. This study considers SCFCL with impedance jX_{fcl} at three possible locations L1, L2, and L3, as shown in Fig. 1.

1) Change in Network Impedance: Table I presents the modified network with SCFCL impedance at various locations and respective X_{tra} expressions during fault and post-fault periods. The values of X_{tra} for various SCFCL locations are compared with that for the network without SCFCL to comment on the changes in P^{f}_{max} and P^{pf}_{max} due to the SCFCL impedance. The values of X_{tra} during fault with SCFCL at locations L1 and L2 are higher than those with no SCFCL. This X_{tra} in fault period suggests a reduction in P^{f}_{max} due to SCFCL at L1 and L2. On the other hand, the value of X_{tra} during fault with SCFCL at location L3 is less than that with no SCFCL, which results in higher P^{f}_{max}. These cases suggest that depending on the SCFCL location, it may lead to an increase or decrease in the P^{f}_{max}, as shown in Fig. 1. Similar analysis of X_{tra} in the post-fault period suggests that the SCFCL impedance increases X_{tra} for locations L1 and L2 from that with no SCFCL. This X_{tra} results in a reduction in P^{pf}_{max}. For SCFCL at location L3, X_{tra} in the post fault period remains the same as that with no SCFCL suggesting no change in P^{pf}_{max}. These cases suggest that the presence of SCFCL

TABLE I
EFFECTIVE NETWORK IMPEDANCE WITH SCFCL AT VARIOUS LOCATIONS

Location	Fault period		Post-fault period	
	Network	Expression	Network	Expression
No SCFCL	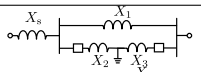	$\frac{X_s X_1}{X_2} + X_s + X_1$	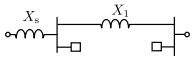	$X_s + X_1$
L1	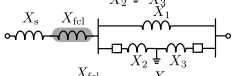	$\frac{X_s X_1}{X_2} + X_s + X_1 + X_{fcl}(1 + \frac{X_1}{X_2})$	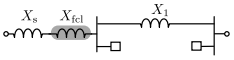	$X_s + X_1 + X_{fcl}$
L2	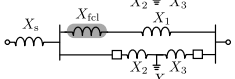	$\frac{X_s X_1}{X_2} + X_s + X_1 + X_{fcl}(1 + \frac{X_s}{X_2})$	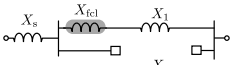	$X_s + X_1 + X_{fcl}$
L3	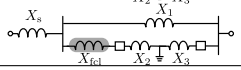	$\frac{X_s X_1}{X_2} + X_s + X_1 - \frac{X_{fcl} X_1 X_s}{X_2(X_2+X_{fcl})}$	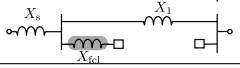	$X_s + X_1$

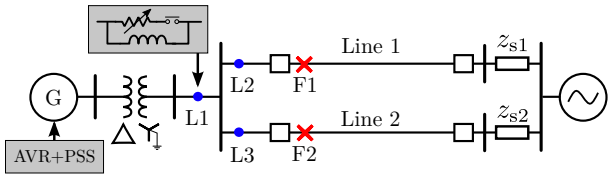

Fig. 3. Test System

impedance in the post-fault period may lead to a decrease in the P^{pf}_{max}, as shown in Fig. 1

2) Critical Clearing Time: Any decrease in δ_{cr} indicates a reduction in the critical clearing time of the faulted element to ensure rotor angle stability. The modified critical clearing angle due to SCFCL impedance (δ^s_{cr}) can be calculated using (3) by substituting the modified P_{max} values. For SCFCL installation at L3, the SCFCL activation only decreases the accelerating area, resulting in $\delta^s_{cr} > \delta_{cr}$ or increased critical clearing time. For SCFCL installation at L1 and L2, the SCFCL modifies both P^f_{max} and P^{pf}_{max}. Hence, a condition is derived from (3) for $\delta^s_{cr} < \delta_{cr}$ as (4). The SCFCL installation satisfying (4) for a faulted element reduces its critical clearing time.

$$P^f_{max} < \frac{P_m(\delta_m - \delta_0) + P^{pf}_{max}(\cos\delta_m - \cos\delta_{cr})}{\cos\delta_0 - \cos\delta_{cr}} \quad (4)$$

The impacts of the SCFCL with delayed recovery on the transient rotor angle stability discussed above are tested using time-domain simulations with detailed models.

III. TEST SYSTEM

A single-machine infinite bus system is chosen to demonstrate the impact on transient stability due to SCFCLs with delayed recovery. Fig. 3 shows the single-line diagram of the test system, consisting of a synchronous generator connected to an infinite bus through two parallel transmission lines. The study employs EMTP-ATP to conduct time-domain simulations with a detailed model of SCFCL. This study requires time-domain modeling, as the activation of the SCFCL depends on the instantaneous value of the fault current component flowing through it.

Table II presents the test system data [27] and synchronous machine data [26], reproduced here for convenience. The generator model considers a Type 58 synchronous machine,

TABLE II
DATA FOR TEST SYSTEM

Element	Parameters
Generator	1000 MVA, 20 kV, $R_a = 0.003$, $X_l = 0.15$, $X_0 = 0.04$, $X_d = 1.81$, $X'_d = 0.3$, $X''_d = 0.25$, $X_q = 1.76$, $X'_q = 0.65$, $X''_q = 0.25$, $T'_{do} = 8$ s, $T''_{do} = 0.03$ s, $T'_{qo} = 1$ s, $T''_{qo} = 0.07$ s, $H = 3.5$ (all impedances in pu)
Transformer	1000 MVA, 20/230 kV, $z_t = 0.017 + j0.138$ pu
Line 1	$z^{00} = 8.129 + j40.988\ \Omega$, $z^{01} = 3.252 + j16.395\ \Omega$
Line 2	$z^{00} = 1.725 + j12.138\ \Omega$, $z^{01} = 0.508 + j3.57\ \Omega$
Source	230 kV, $z_{s1} = j3.87\ \Omega$, $z_{s2} = j6.05\ \Omega$

and its excitation system considers a type ST1A excitation system with an automatic voltage regulator (AVR) and a power system stabilizer (PSS) [26]. The speed governor effects are neglected for this study. The generator transformer is modeled as a saturable transformer with delta connection at the generator side and solidly grounded star connection at the transmission network side. Table II presents the data for the generator transformer. The transmission lines are modeled with series lumped parameters for the transient stability study, with zero and positive sequence impedances given in Table II. The infinite bus is modeled as a constant voltage source and impedance with the values given in Table II. Each transmission line is equipped with circuit breakers at both ends to ensure fault-clearing by three-pole operation for any fault type. The circuit breakers are modeled as ideal switches which trip at current zeroes.

This study focuses on the resistive SCFCL, which is also compared with two SCFCLs available in the literature. For a fair comparison, the parameters of these SCFCLs are kept the same. The SCFCLs are considered with a critical current rating of 4.5 kA, impedance after activation of 10 Ω, and recovery time of 10 s. The considered SCFCLs and their modeling in EMTP-ATP are briefly discussed below.

1) Resistive SCFCL: Fig. 2a shows the resistive SCFCL with a shunt reactor in a phase. The SCFCL employs the superconducting (SC) element to limit the fault current, which transitions to a high impedance state for currents higher than its critical current rating. After this transition, the quenched SC element is disconnected from the circuit using a load break switch. The load break switch remains open for a predetermined period to ensure the successful recovery of the SC element. The SC element is modeled using a model based

on the E-J power law for YBCO (yttrium barium copper oxide) superconducting tape-based SC element [24]. The load break switches are modeled as ideal switches, and the shunt reactor is modeled as pure inductor. This SC element defines the SCFCL critical current and recovery time, and the shunt reactor with $X_{\text{fcl}} = 10\ \Omega$ defines the SCFCL impedance.

In addition, this study considers two modes of load break switch operation, namely individual phase operation and gang operation. Only load break switches in faulted phases are operated in individual phase activation mode following an asymmetrical fault. All the load break switches are operated in gang operation irrespective of the fault type. Both these modes are considered since the circuit breaker operation practices vary according to utility practices. The performance of these modes is similar in the case of a three phases fault.

2) Air coil SCFCL: A phase of the air coil SCFCL consists of a short-circuited SC element coil inserted into an air core reactor, forming the primary to SC element secondary [28]. Fig. 2b shows the circuit representation of the air coil SCFCL, where the air core transformer accounts for mutual and leakage inductance of the coils. The SC element has negligible resistance during normal operation, in which case the small leakage inductance and resistance of the primary reactor define the SCFCL impedance. The quenched SC element during fault increases the secondary impedance, in which case the magnetizing branch of the air core transformer dominates the SCFCL impedance [28].

Each phase of the air core SCFCL is modeled as a transformer with an SC element connected at the secondary [29]. The transformer and SC element parameters to provide $10\ \Omega$ impedance during fault are derived from an air coil SCFCL for medium voltage applications [29]. The air coil SCFCL has an impedance of $0.04+j1.15\ \Omega$ and $\approx 3.38+j9.42\ \Omega$ during normal operation and fault conditions, respectively. The air coil SCFCL remains in the high impedance state during the post-fault period due to the finite recovery time of the SC element.

3) Quick Recovery SCFCL: Unlike previous SCFCLS, a quick recovery SCFCL is expected to provide negligible impedance when the fault is cleared. For this study, the resistive SCFCL with two branches of SC element with load break switch arrangement is considered as an example of quick recovery SCFCL [9], [17]. The load break switch in series with the second SC element is usually kept open and closed after the fault clearing. Its working principle and modeling are similar to the resistive SCFCL. Furthermore, non-quench-type SCFCLs and solid-state FCLs (such as [30]) with quick recovery can be investigated similarly to the quick recovery SCFCL considered here.

IV. Simulation Results and Discussions

This section presents the assessment of the transient rotor angle stability based on time-domain simulations. The simulation setup considers the initial condition of the synchronous generator supplying 900 MW to the network at the terminal voltage of $1.05\angle 13°$ pu. The fault is simulated at $t = 0.495$ s, and it is assumed that the protection system detects the fault under the influence of the SCFCL. The fault is cleared at $t = 0.495 + T_{\text{c}}$ by the three-pole operation of the circuit breakers at both ends of the faulted line, where T_{c} is the fault clearing time. The generator response is studied for the SCFCL locations defined in the test cases by varying the fault clearing time, the SCFCL impedance, and the fault type.

TABLE III
Test Cases Based on SCFCL Locations

Case	SCFCL		Fault	
	Type	Location	Type	Location
Case A	No SCFCL	-	3 phase	F2
Case B	Resistive	L1	3 phase	F2
Case C	Resistive	L2	3 phase	F2
Case D	Resistive	L3	3 phase	F2

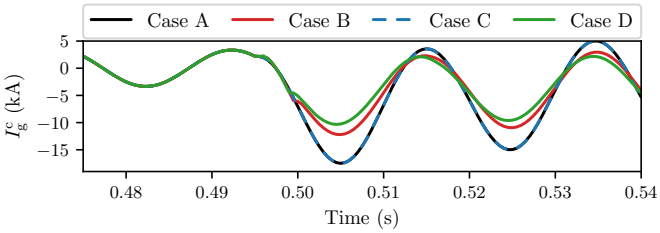

Fig. 4. Phase C current at high voltage side of the generator-transformer for various test cases.

A. Transient Stability with Different SCFCL Locations

This exercise aims to develop an understanding of the transient stability of the system with SCFCL with delayed recovery. The exercise considers the system with the resistive SCFCL for a solidly grounded three-phase fault at location F2 near the circuit breaker of Line 2, as shown in Fig. 3. The generator response following an SCFCL activation is analyzed based on the generator power output (P_{e}), its relative speed ($\Delta\omega = \omega_{\text{g}} - \omega_{\text{s}}$), and its rotor angle ($\delta$). Fig. 4 shows the pre-fault generator current of 2.37 kA at the high-voltage side of the generator-transformer. Fig. 5 shows the initial value of generator angle $\delta_0 = 25.36°$ for delivering $P_{\text{e}} = 900$ MW in the pre-fault period. This pre-fault condition is common for all test cases. The following discussion considers clearing time $T_{\text{c}} = 200$ ms for all the test cases.

1) Case A: This base case does not consider SCFCL installation in the network. The solidly grounded three-phase fault close to the terminals of the generator-transformer has contributions from the generator and the infinite bus through Line 1 and Line 2. Fig. 4 shows the phase C of the generator contribution, which has a peak of -17.50 kA. Fig. 5 shows the drop in P_{e} in the fault period due to the solidly ground fault. The generator power during fault is negligible, as there is no active power transfer to the infinite bus. Fig. 5 shows an acceleration of the rotor (increase in $\Delta\omega$) during the fault period, resulting from the mismatch between constant generator input and output.

The circuit breakers of the faulted line open at $t = 0.695$ s. The successful clearing of the faulted line increases the $P_{\text{max}}^{\text{pf}}$. Eq. (1) gives a numerical value of $P_{\text{max}}^{\text{pf}} = 1383$ MW. The

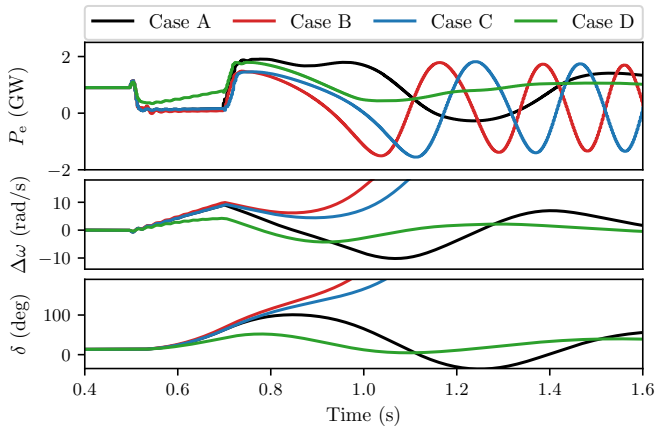

Fig. 5. Generator response to a solid three phase fault at F2 cleared after 200 ms for various test cases.

TABLE IV
TEST CASES WITH DIFFERENT SCFCLS

Case	SCFCL		Fault	
	Type	Location	Type	Location
Case A	No SCFCL	-	3 phase	F2
Case B	Resistive	L1	3 phase	F2
Case E	Air coil	L1	3 phase	F2
Case F	Quick rec.	L1	3 phase	F2

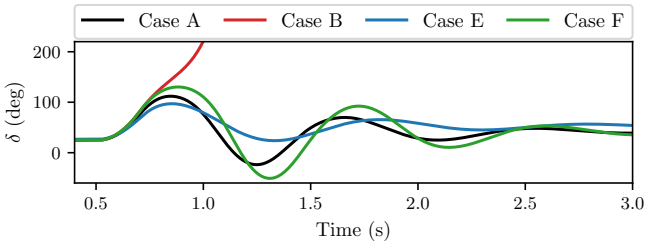

Fig. 6. Rotor angle response with different SCFCLs.

increased P_e in the post-fault period leads to deceleration of the rotor, as seen in Fig. 5. Fig. 5 suggests that the generator is first-swing stable for the fault-clearing after 200 ms.

2) Case B: This case considers SCFCL installation in series with the generator-transformer. The fault leads to SCFCL activation since the fault contribution from the generator is higher than the SCFCL critical current rating. Fig. 4 shows the phase C generator current reduction from the projected peak of -17.50 kA to -12.18 kA due to the SCFCL activation. Fig. 5 shows negligible P_e delivered in the fault period. The SCFCL installation limits the fault contribution from the generator; however, it does not increase the P_e during the fault period. Fig. 5 shows rotor acceleration during the fault period due to the mismatch between generator input and output power.

After clearing the fault, the SCFCL maintains high impedance until its predefined recovery time. SCFCL impedance in the post-fault period increases the network impedance, reducing P^{pf}_{max} from 1383 MW in Case A to 1124 MW. Fig. 5 shows that the value of P_e in Case B is lower than in Case A. The lower value of P^{pf}_{max} leads to further rotor acceleration, eventually leading to first-swing instability. Fig. 4 and Fig. 5 suggest that even though the SCFCL installation limits the fault contribution, its high impedance in the post-fault period adversely impacts the rotor angle stability.

3) Case C: This case considers SCFCL installation in series with Line 1. The fault leads to a higher fault current contribution from the infinite bus through Line 1 than the SCFCL critical current rating, which activates it. The SCFCL impedance limits the current contribution from Line 1; however, the current contribution from the generator remains unchanged. Fig. 4 shows the generator current for Case C, similar to that in Case A. Fig. 5 shows the generator response in terms of P_e, and rotor acceleration during fault is similar to that in Case A.

For this case, the SCFCL remains in a high impedance state in the post-fault network resulting in $P^{pf}_{max} = 1124$ MW, similar to that in Case B. The generator is first-swing unstable due to the increased network impedance post-fault. The SCFCL installation does not limit the generator fault current contribution, and its impedance in the post-fault period adversely impacts the rotor angle stability.

4) Case D: This case considers SCFCL installation in series with Line 2. For this case, the SCFCL carries the fault current contributions from the generator and Line 1. For the simulated fault, this contribution is higher than its critical current rating leading to its activation. Fig. 4 shows the reduction in the peak of fault contribution from the generator to -10.09 kA. The SCFCL impedance helps increase P_e during the fault period, as seen in Fig. 5. This power transfer during fault results in lower rotor acceleration than Case A.

As the SCFCL is in series with Line 1, clearing it also disconnects the SCFCL from the network. Irrespective of the SCFCL recovery, its impedance does not increase network impedance in the post-fault period. The P^{pf}_{max} for the case is 1383 MW, similar to Case A, and leads to deceleration of the rotor. Fig. 5 shows a stable operation for this case. The SCFCL installation limits the generator fault contribution and improves the rotor angle stability.

B. Transient Stability with Different SCFCLs

Here the transient rotor angle stability of the system with resistive SCFCL is compared with other SCFCLs. Table IV presents the test cases defined with different SCFCLs for the same location and fault. Fig. 6 shows the rotor angle response with different SCFCLs for the fault at $t = 0.495$ s is cleared after 200 ms. As discussed earlier, the generator is first-swing stable for Case A and unstable for Case B. In Case B, the resistive SCFCL injects an impedance of $j10\ \Omega$ in fault and post-fault periods.

For Case E, the fault current contribution through the air coil SCFCL leads to the quenching of the SC element in each phase. After transitioning to the high impedance state, the air coil SCFCL injects an impedance of $\approx 3.38 + j9.42\ \Omega$ during fault and post-fault periods. Fig. 6 shows that the generator is first-swing stable for the system with air coil SCFCL. As seen in Case B, the fault current contribution through quick recovery SCFCL leads to its activation. The SCFCL injects an impedance of $j10\ \Omega$ during fault. After 20 ms from the fault clearing, the load break switch of the second branch

TABLE V
CRITICAL CLEARING TIMES (IN MS)

Fault	No SCFCL	Resisitive			Air coil		
		L1	L2	L3	L1	L2	L3
F1	234	195	>500	206	278	>500	226
F2	222	177	189	>500	256	209	>500

of SC element is closed. This switching reduces the SCFCL impedance to a negligible value in post-fault period. Fig. 6 shows that the change in rotor angle for Case F is similar to that in Case B up to $t = 0.715$ s. The rotor deceleration after the quick recovery of the SCFCL leads to the first-swing stable generator operation. Fig. 6 shows that the rotor angle oscillations are less in the case of air coil SCFCL followed by in the system without SCFCL and with quick recovery SCFCL.

As discussed in Section I, the literature consists of multiple studies involving quick recovery SCFCLs and hence is not considered in subsequent discussions.

C. Critical Clearing Time for Different SCFCLs

The previous time-domain study is extended to determine the critical clearing times for the three-phase faults at locations F1 and F2. The critical clearing time (T_{cr}) is obtained using a multi-run of the time-domain simulations by varying trip times of the circuit breakers from 100 to 500 ms. Table V presents T_{cr} obtained from the time-domain simulations for three-phase faults at F1 and F2. The T_{cr} values for the system without SCFCL are considered base cases and given as 234 and 222 ms for faults at F1 and F2, respectively. .

For fault at F1, Table V suggests that the resistive SCFCL at locations L1 and L3 reduce T_{cr} from base case to 195 and 206 ms, respectively. For the same fault, the resistive SCFCL at location L2 increase T_{cr} beyond 500 ms. For the fault at F2, the resistive SCFCL at location L3 increases T_{cr} beyond 500 ms and that at locations L1 and L2 reduces T_{cr} to 177 and 189 ms, respectively. The cases where the resistive SCFCL with high impedance remains in the post-fault period observe a reduction in T_{cr}. The air coil SCFCL installation at location L1 observes an increase in T_{cr} to 278 ms for fault at F1 and 256 ms for fault at F2 from respective base cases. For location L2, the air coil SCFCL installation increases T_{cr} for fault at F1 beyond 500 ms and decreases for fault at F2 to 209 ms. Similarly, the air coil SCFCL at location L3 increases T_{cr} for fault at F2 beyond 500 ms and decreases for fault at F1 to 226 ms. It is observed that the system with air coil SCFCL has higher T_{cr} as compared to those for the resistive SCFCL.

D. Change in SCFCL impedance

This exercise aims to identify the impact of change in SCFCL impedance on the rotor angle stability. For this demonstration, the SCFCL impedance X_{fcl} is varied to 0 Ω, 5 Ω, 10 Ω, and 15 Ω for Cases B-D in Table III. The parameters of the SC element are kept constant, suggesting the same critical current rating and recovery time. The fault is simulated at $t = 0.495$ s with $T_{\text{c}} = 200$ ms. Fig. 7 shows that all test cases with $X_{\text{fcl}} = 0$ Ω lead to stable operation.

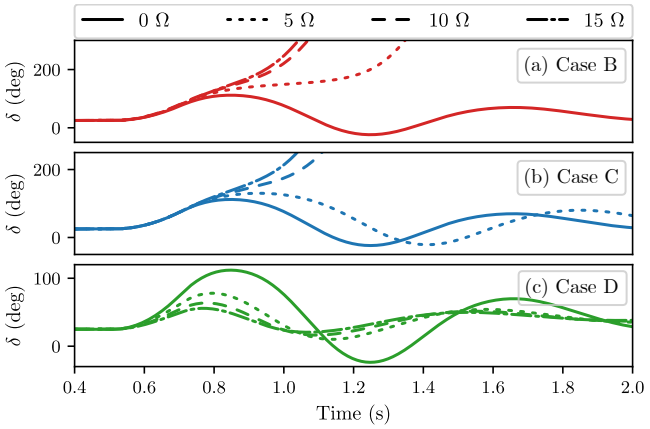

Fig. 7. Change in rotor angle response with change in SCFCL impedance for various test cases.

TABLE VI
TEST CASES FOR ASYMMETRICAL FAULTS WITH DIFFERENT SCFCLS

Case	SCFCL		Fault	
	Type	Location	Type	Location
Case G	No SCFCL	L1/L2	SLG/DLG	F2
Case H	Resistive (Indi.)	L1/L2	SLG/DLG	F2
Case I	Resistive (Gang)	L1/L2	SLG/DLG	F2
Case J	Air coil	L1/L2	SLG/DLG	F2

Fig. 7a shows first-swing instability for Case B with X_{fcl} =5, 10, and 15 Ω. The rising rate of δ is higher for higher values of X_{fcl}. A similar increase in the rising rate of δ is observed in Fig. 7b for Case C with the increase in X_{fcl}. Fig. 7b shows that the generator operation is stable with $X_{\text{fcl}} = 5$ Ω and unstable with X_{fcl} =10 and 15 Ω for Case C. For Case D, Fig. 7c shows the generator is first-swing stable for all considered X_{fcl} values. Fig. 7c also shows a reduction in rotor angle oscillations with the increase in X_{fcl} value.

E. Performance During Asymmetrical Faults

This exercise aims to find the change in $P^{\text{pf}}_{\text{max}}$ due to the activation of SCFCL following asymmetrical faults. The changes in $P^{\text{pf}}_{\text{max}}$ can be identified from the post-fault equilibrium condition $P_{\text{m}} = P^{\text{pf}}_{\text{max}} \sin \delta^{\text{new}}$, where a constant P_{m} with higher δ^{new} suggests a reduction in $P^{\text{pf}}_{\text{max}}$. Table VI presents the test cases defined with three SCFCLs consisting air coil SCFCL and resistive SCFCL with individual and gang operation of load break switches. The study considers single-line-to-ground (SLG) fault in phase A and double-line-to-ground (DLG) fault involving phases B and C. These asymmetrical faults are simulated at F2 at $t = 0.495$ s and are cleared after 200 ms by disconnecting the faulted line with three pole tripping of circuit breakers.

1) Location L1: The SCFCL at location L1 carries currents from the generator which may see increase in healthy phase currents following asymmetrical faults due to coupling. Fig. 8 shows these phase currents following asymmetrical faults in Case G. For the SLG fault, Fig. 8a shows an increase in the faulted phase A and healthy phase B currents beyond SCFCL critical current rating. These currents quench the SC elements in phases A and B for the fault in phase A. Similarly, Fig. 8b

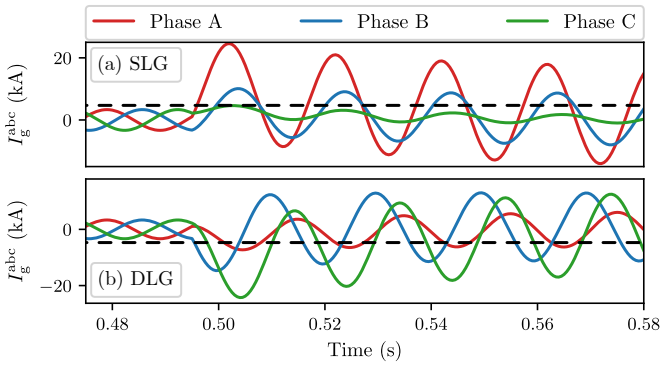

Fig. 8. Phase currents at high voltage side of the generator transformer for Case G.

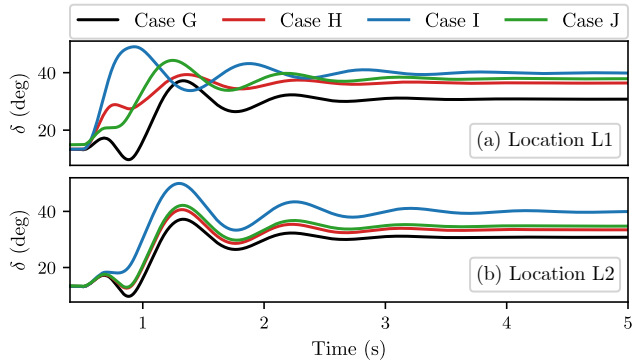

Fig. 9. Rotor angle response for a SLG fault at F1 cleared after 200 ms.

shows an increase in all phases beyond SCFCL critical current rating for the DLG fault quenching SC element in all phases. Fig. 9a shows the rotor angle response following the SLG for Cases G-J with SCFCL at location L1. The SCFCL injects impedance in phases A and B for Cases H and J and in all the phases for Case I. The values of δ^{new} in Fig. 9a suggest that the $P^{\text{pf}}_{\text{max}}$ is highest in Case G, followed by that in Cases H and J, and is lowest in Case I due to SCFCL impedance insertion in all three phases. Fig. 10a shows the rotor angle response following the DLG for Cases G-J with SCFCL at location L1. Cases H-J observe a negligible difference in δ^{new} values, resulting from similar SCFCL impedance injection in Cases H-J. The values of δ^{new} in Fig. 10a suggest a reduction in $P^{\text{pf}}_{\text{max}}$ due to SCFCL impedance in Cases H-J as compared to Case G.

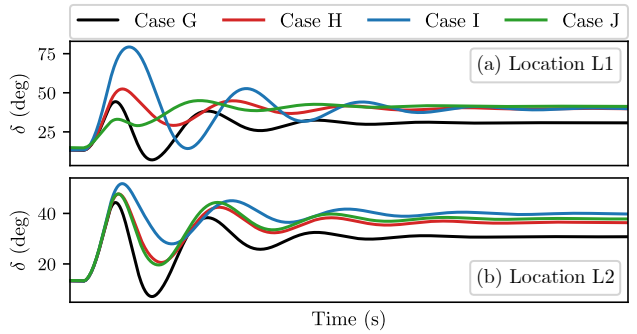

Fig. 10. Rotor angle response for a DLG fault at F1 cleared after 200 ms.

2) Location L2: The asymmetrical faults at F2 observe Line 1 currents higher than SCFCL critical current only in the faulted phases. Hence, the asymmetrical faults lead to SC element quenching only in the faulted phases for SCFCL installations at location L2. The δ^{new} in Fig. 9b suggests that the $P^{\text{pf}}_{\text{max}}$ is higher for Cases H and J with impedance injection in single phase than for Case I with impedance injection in all phases. Similarly, Fig. 10b suggests higher $P^{\text{pf}}_{\text{max}}$ for Cases H and J with impedance injection in two phases than in Case I.

F. Discussions

The observations of the time-domain simulation study are summarized as follows:

- The results in Fig. 5 suggest that the resistive SCFCL activation adversely impacts the transient stability for the SCFCL locations where its impedance reduces the power transfer during fault and post-fault periods. Cases B and C observe a reduction in both $P^{\text{f}}_{\text{max}}$ and $P^{\text{pf}}_{\text{max}}$ due to SCFCL activation. For similar cases, Table V shows lower critical clearing times for fault F1 with SCFCL locations L1 and L3 and fault F2 with SCFCL locations L1 and L2. This observation validates the finding of [20], [21] for the test system under study. On the contrary, the increase in $P^{\text{f}}_{\text{max}}$ and no change in $P^{\text{pf}}_{\text{max}}$ for Case D improves the transient stability. Table V shows higher critical clearing time for faults F1 and F2 with SCFCL locations L2 and L3, respectively.
- In addition, the SCFCL with quick recovery reduces only the $P^{\text{f}}_{\text{max}}$ during fault in Case F. A comparison between the rotor angle responses in Fig. 6 suggests that the SCFCL adversely impacts the transient stability in Case F as compared to Case A.
- For the studied Cases B and E as shown in Fig. 6, the air coil SCFCL and resistive SCFCL have similar recovery times. However, Fig. 6 shows stable operation for Case E which has air coil SCFCL as against the unstable operation for Case B which uses resistive SCFCL. The reason for this behaviur being the presence of resistive element in the air coil SCFCL. The impedance for air coil SCFCL was $3.38+j9.42\ \Omega$ whereas that for resistive SCFCL was $j10\ \Omega$. Table V shows higher critical clearing times for air coil SCFCL than resistive SCFCL.
- The adverse impact of SCFCL on rotor angle stability increases with an increase in SCFCL impedance, as seen in Fig. 7.
- The individual phase activation of the SCFCL following an asymmetrical fault, as in Cases H and J, leads to higher power transfer than that in the case of SCFCL with gang activation.

Even though this simulation study use a typical single-machine-infinite-bus with few network faults for demonstration, it bring out the importance of changes in post-fault power transfer due to SCFCL impedance. These findings can be helpful while analyzing the transient stability of any system consisting SCFCL with delayed recovery.

V. Conclusions

This paper explores the impact of SCFCL with delayed recovery on rotor angle stability of the system. The presented mathematical analysis and time-domain simulations for the single-machine infinite-bus system suggest that: 1. The SCFCL activation not always increases $P_{\max}$ in the fault period which depends on SCFCL location, and 2. The SCFCL impedance during recovery reduces $P_{\max}$ in the post-fault period. For the SCFCL locations considered in the study, the results show that the presence of SCFCL impedance in the post-fault period adversely impact the transient stability resulting lower critical clearing times. It is observed the resistive element in SCFCL impedance may lead to an increase in critical clearing time, which indicates increased transient stability. The simulation study also shows that the post-fault power transfer can be increased with individual phase activation in case of asymmetrical faults.

References

[1] W. G. 23.03, "TB 214: The mechanical effects of short circuit curretns in open air substations (Part II)," *CIGRE*, Oct. 2002.

[2] S. Kodle, V. Padmini *et al.*, "Application of super conducting fault current limiter in indian grid," in *IEEE 6th International Conference on Power Systems (ICPS)*. IEEE, 2016, pp. 1–6.

[3] B. Li, C. Li, and F. Guo, "Application studies on the active sisfcl in electric transmission system and its impact on line distance protection," *IEEE Trans. Appl. Supercond.*, vol. 25, no. 2, pp. 1–9, 2014.

[4] W. T. B. De Sousa, T. M. L. Assis *et al.*, "Simulation of a superconducting fault current limiter: A case study in the brazilian power system with possible recovery under load," *IEEE Trans. Appl. Supercond.*, vol. 26, no. 2, pp. 1–8, 2015.

[5] B. Li, C. Li *et al.*, "Overcurrent protection coordination in a power distribution network with the active superconductive fault current limiter," *IEEE Trans. Appl. Supercond.*, vol. 24, no. 5, pp. 1–4, 2014.

[6] J.-S. Kim, S.-H. Lim, and J.-C. Kim, "Study on application method of superconducting fault current limiter for protection coordination of protective devices in a power distribution system," *IEEE Trans. Appl. Supercond.*, vol. 22, no. 3, pp. 5 601 504–5 601 504, 2011.

[7] S.-H. Lim and S.-T. Lim, "Analysis on coordination of over-current relay using voltage component in a power distribution system with a sfcl," *IEEE Trans. Appl. Supercond.*, vol. 29, no. 5, pp. 1–5, 2019.

[8] B. C. Sung, D. K. Park *et al.*, "Study on a series resistive sfcl to improve power system transient stability: modeling, simulation, and experimental verification," *IEEE Trans. Ind. Electron.*, vol. 56, no. 7, pp. 2412–2419, 2009.

[9] M. Tsuda, Y. Mitani *et al.*, "Application of resistor based superconducting fault current limiter to enhancement of power system transient stability," *IEEE Trans. Appl. Supercond.*, vol. 11, no. 1, pp. 2122–2125, 2001.

[10] B. C. Sung, D. K. Park *et al.*, "Study on optimal location of a resistive sfcl applied to an electric power grid," *IEEE Trans. Appl. Supercond.*, vol. 19, no. 3, pp. 2048–2052, 2009.

[11] L. Chen, Y. Tang *et al.*, "Influence of a voltage compensation type active superconducting fault current limiter on the transient stability of power system," *Physica C: Superconductivity*, vol. 469, no. 15-20, pp. 1760–1764, 2009.

[12] G. Didier, J. Leveque, and A. Rezzoug, "A novel approach to determine the optimal location of sfcl in electric power grid to improve power system stability," *IEEE Trans. Power Syst.*, vol. 28, no. 2, pp. 978–984, 2012.

[13] G. Didier and J. Lévêque, "Influence of fault type on the optimal location of superconducting fault current limiter in electrical power grid," *International Journal of Electrical Power & Energy Systems*, vol. 56, pp. 279–285, 2014.

[14] M. Sjostrom, R. Cherkaoui, and B. Dutoit, "Enhancement of power system transient stability using superconducting fault current limiters," *IEEE Trans. Appl. Supercond.*, vol. 9, no. 2, pp. 1328–1330, 1999.

[15] Y. Goto, K. Yukita *et al.*, "A study on power system transient stability due to introduction of superconducting fault current limiters," in *International Conference on Power System Technology*, vol. 1. IEEE, 2000, pp. 275–280.

[16] L. Chen, J. Tang *et al.*, "Study of resistive superconducting fault current limiters for stability improvement of vsg-controlled multiple microgrid clusters," *IEEE Trans. Appl. Supercond.*, vol. 32, no. 4, pp. 1–7, 2022.

[17] I. Hwang, S. R. Lee *et al.*, "Improvement of the transient stability using sfcl in korean power systems," *Physica C: Superconductivity*, vol. 494, pp. 335–338, 2013.

[18] S. Seo, S.-J. Kim *et al.*, "A hybrid superconducting fault current limiter for enhancing transient stability in korean power systems," *Physica C: Superconductivity*, vol. 494, pp. 331–334, 2013.

[19] M. M. Hossain and M. H. Ali, "Transient stability improvement of doubly fed induction generator based variable speed wind generator using dc resistive fault current limiter," *IET Renewable Power Generation*, vol. 10, no. 2, pp. 150–157, 2016.

[20] W. G. A3.23, "TB 497: Application and feasibility of fault current limiters in powers systems," *CIGRE*, Jun. 2012.

[21] V. Sokolovsky, V. Meerovich, and I. Vajda, "Transient stability of a power system with superconducting fault current limiters," *Electrical Engineering*, vol. 51, pp. 3–9, 2007.

[22] P. Tixador, *Superconducting Fault Current Limiter: Innovation for the Electric Grids*. World Scientific, 2018.

[23] W. Chen, P. Song *et al.*, "Investigations on quench recovery characteristics of high-temperature superconducting coated conductors for superconducting fault current limiters," *Electronics*, vol. 10, no. 3, p. 259, 2021.

[24] E. Egorova, H. Bahirat *et al.*, "Emtp-atp modeling of a resistive superconducting fault current limiter," in *International Conference on Power Systems Transients (IPST2013), Vancouver, Canada*, 2013.

[25] M. Moyzykh, D. Gorbunova *et al.*, "First Russian 220 kV superconducting fault current limiter (SFCL) for application in city grid," *IEEE Trans. Appl. Supercond.*, vol. 31, no. 5, pp. 1–7, 2021.

[26] P. Kundur, *Power system stability and control*. McGraw-Hill Education (India), New Delhi, 1994.

[27] J. A. Martinez-Velasco, *Transient Analysis of Power Systems: A Practical Approach*. John Wiley & Sons, 2020.

[28] A. Kudymow, A. Bauer *et al.*, "Smartcoil—design, assembly and test of a 10 mva superconducting air coil fault current limiter," *Superconductor Science and Technology*, vol. 32, no. 6, p. 065002, 2019.

[29] W. De Sousa, A. Polasek *et al.*, "Simulations of resistive and air coil sfcls in a power grid," *IEEE Trans. Appl. Supercond.*, vol. 25, no. 3, pp. 1–5, 2015.

[30] M. E. Hossain, "A non-linear controller based new bridge type fault current limiter for transient stability enhancement of dfig based wind farm," *Electric Power Systems Research*, vol. 152, pp. 466–484, 2017.